JOURNAL OF PETROLOGY | VOLUME 43 | NUMBER 12 | PAGES 2261–2278 | 2002

Sr–Nd–Pb Isotopic Compositions of Peridotite Xenoliths from Spitsbergen: Numerical Modelling Indicates Sr–Nd Decoupling in the Mantle by Melt Percolation Metasomatism

DMITRI A. IONOV[1,2]*, SAMUEL B. MUKASA[3] AND JEAN-LOUIS BODINIER[4]

[1]DEPARTMENT OF EARTH AND ENVIRONMENTAL SCIENCES, UNIVERSITÉ LIBRE DE BRUXELLES CP160/02, B-1050 BRUSSELS, BELGIUM

[2]DEPARTEMENT DE GÉOLOGIE, UNIVERSITÉ JEAN MONNET, ST-ETIENNE F-42023, FRANCE

[3]DEPARTMENT OF GEOLOGICAL SCIENCES, UNIVERSITY OF MICHIGAN, ANN ARBOR, MI 48109-1063, USA

[4]LABORATOIRE DE TECTONOPHYSIQUE (UMR 5568 CNRS), ISTEEM, UNIVERSITÉ MONTPELLIER 2, CASE 057, 34095 MONTPELLIER CEDEX 05, FRANCE

RECEIVED OCTOBER 2, 2000; REVISED TYPESCRIPT ACCEPTED MAY 22, 2002

Several spinel peridotite xenoliths from Spitsbergen have Sr–Nd isotopic compositions that plot to the right of the 'mantle array' defined by oceanic basalts and the DM end-member (depleted mantle, with low $^{87}Sr/^{86}Sr$ and high $^{143}Nd/^{144}Nd$). These xenoliths also show strong fractionation of elements with similar compatibility (e.g. high La/Ce), which cannot be produced by simple mixing of light rare earth element-depleted peridotites with ocean island basalt-type or other enriched mantle melts. Numerical simulations of porous melt flow in spinel peridotites applied to Sr–Nd isotope compositions indicate that these features of the Spitsbergen peridotites can be explained by chemical fractionation during metasomatism in the mantle. 'Chromatographic' effects of melt percolation create a transient zone where the host depleted peridotites have experienced enrichment in Sr (with a radiogenic isotope composition) but not in Nd, thus producing Sr–Nd decoupling mainly controlled by partition coefficients and abundances of Sr and Nd in the melt and the peridotite. Therefore, Sr–Nd isotope decoupling, earlier reported for some other mantle peridotites worldwide, may be a signature of metasomatic processes rather than a source-related characteristic, contrary to models that invoke mixing with hypothetical Sr-rich fluids derived from subducted oceanic lithosphere. Pb isotope compositions of the Spitsbergen xenoliths do not appear to be consistently affected by the metasomatism.

KEY WORDS: *Spitsbergen; lithospheric mantle; metasomatism; radiogenic isotopes; theoretical modelling*

INTRODUCTION

Spinel peridotite xenoliths from the island of Spitsbergen in the North Atlantic are fragments of continental upper mantle located at present in the extreme northwest of the Eurasian continent, near a lithospheric plate boundary created by recent oceanic spreading (Fig. 1). Here we report Sr–Nd–Pb isotope data for the same samples that were the subject of a detailed major and trace element study (Ionov *et al.*, 2002). The geochemistry of the Spitsbergen xenolith suite indicates an origin for most rocks as residues after moderate to high degrees of partial

*To whom correspondence should be addressed at present address: Laboratoire de Tectonophysique, ISTEEM, CNRS & Université Montpellier 2, case 049, 34095 Montpellier cedex 05, France. Telephone: +33-467143602. Fax: +33-467143603. E-mail: ionov@dstu.univ-montp2.fr

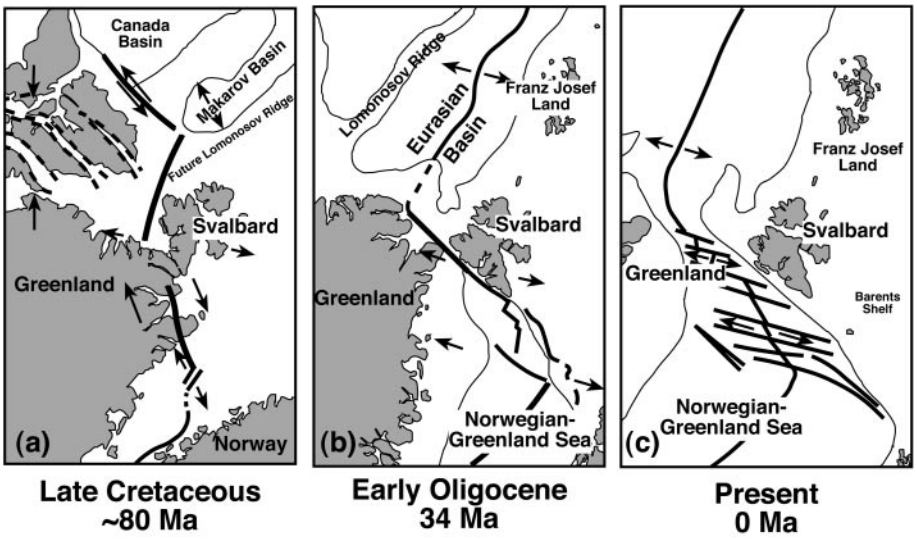

Fig. 1. Tectonic reconstructions for Svalbard and the NW Atlantic modified from Blythe & Kleinspehn (1998). Bold lines indicate positions of major fracture zones.

melting and melt extraction. Quantitative estimates based on mineral–melt equilibria and numerical simulation of porous melt flow in peridotites indicate that the partial melting residues were subsequently metasomatized by percolation of a melt or fluid enriched in highly incompatible elements (Ionov *et al.*, 2002). The inferences from the trace element study are directly relevant to the interpretation of the radiogenic isotope data.

A major objective of this work is to establish radiogenic isotope signatures of the peridotite mantle beneath Spitsbergen through analysis of the minerals that largely control the budget of Sr, Nd and Pb in spinel peridotites. These data shed light on the origin and evolution of the continental mantle beneath Spitsbergen (formerly a part of northern Laurentia) and globally. Another major goal of this study is to further investigate the impact of mantle metasomatism on radiogenic isotope composition of the lithospheric mantle and define the sources of the metasomatic components.

Mechanisms of mantle metasomatism have been widely debated ever since the broad impact of that phenomenon on lithospheric mantle geochemistry became apparent (e.g. Menzies & Hawkesworth, 1987). The geochemical study of the Spitsbergen xenolith suite (Ionov *et al.*, 2002) together with theoretical modelling has provided evidence for chemical fractionation in the mantle during metasomatism by porous melt flow but did not consider the consequences of those processes for isotopic compositions. Here we address the possible effects of percolation of an enriched melt or fluid in depleted peridotites by applying numerical simulations of those processes to the radiogenic isotope dataset for the Spitsbergen samples, and incorporating relevant literature data for comparisons. A particular challenge in this study is to provide a model of metasomatism that is quantitatively consistent with both trace element and radiogenic isotope data for the xenoliths.

The radiogenic isotopes provide an important tool to constrain the sources of melts and fluids responsible for mantle metasomatism. For example, they can be applied to distinguish between metasomatic media derived from convecting asthenospheric mantle versus subducted oceanic lithosphere. With less certainty, they can also be used to indicate possible provenances within the lithospheric mantle and/or deep-mantle plumes (e.g. Vidal *et al.*, 1989; Tatsumoto *et al.*, 1992; Beard & Glazner, 1995; Carignan *et al.*, 1996; Wiechert *et al.*, 1997; Zangana *et al.*, 1997; Mattielli *et al.*, 1999; Beccaluva *et al.*, 2001; Churikova *et al.*, 2001). On the other hand, porous melt flow also can affect both abundances of the parent–daughter element pairs and radiogenic isotope relationships in the metasomatized mantle (Navon & Stolper, 1987; Reiners, 1998). We specifically aim here to distinguish between the melt percolation effects and the signatures of the melt source in the Sr–Nd isotopic compositions of the lithospheric mantle beneath Spitsbergen and elsewhere.

GEOLOGICAL SETTING AND SAMPLES

The island of Spitsbergen is part of the Svalbard archipelago off Norway between the North Atlantic and Arctic oceanic basins. Svalbard was part of the Laurasian continental platform contiguous with Greenland until the

northward progression of the North Atlantic opening produced Late Cretaceous–Neogene separation of Eurasia and North America (Blythe & Kleinspehn, 1998) (Fig. 1). This separation between Svalbard and Greenland occurred initially along an intra-continental dextral transform fault connecting spreading ridges in the Arctic and Norwegian–Greenland oceanic basins. Episodes of transpression and transtension along the transform plate boundary led to the formation of the Late Cretaceous–Paleogene Spitsbergen Orogen and associated sedimentary basins on Spitsbergen (Amundsen *et al.*, 1987; Blythe & Kleinspehn, 1998). The Atlantic mid-ocean ridge (MOR) propagated northward between Svalbard and Greenland in Oligocene–Miocene times, with coeval volcanic activity on the Yermak Plateau north of Svalbard (Amundsen *et al.*, 1987; Blythe & Kleinspehn, 1998). The xenolith-bearing basaltic rocks on Spitsbergen are located within ~200 km of the North Atlantic MOR.

The xenoliths for this study have been collected in alkali basaltic lavas at three Quaternary volcanic centres in NW Spitsbergen: Sverre, Halvdan and Sigurd. Data on geology, tectonic setting and geophysical results for this region have been summarized by Amundsen *et al.* (1987) and Yevdokimov (2000). Petrographic and chemical data on xenoliths studied in this work have been provided by Ionov *et al.* (1996, 2002).

The xenoliths were cut using a diamond saw; once the rims had been removed, their interiors were crushed in a bench-top jaw crusher, carefully cleaned after each sample to avoid cross-contamination. Aliquots of the crushed samples were ground in an agate mortar to produce whole-rock powders. Another aliquot was sieved and grains were then grouped by size. The 0·2–0·3 mm fraction was separated magnetically to yield sub-fractions enriched in clinopyroxene and amphibole. Ultrapure mineral separates were handpicked from those for isotopic analyses. Several handpicked grains from each sample were put on mounts for *in situ* analyses. The handpicked clinopyroxene grains are larger in size than the clinopyroxene found within the carbonate- and glass-bearing interstitial material (Ionov *et al.*, 1996); the latter therefore are absent from the ultrapure separates analysed for isotopic compositions. Samples of host basalts were sawn off from lava attached to xenoliths. Basalt chips free of saw marks, weathering products and xenocryst material were rinsed in diluted nitric acid and ground to powder in an agate mortar.

Most of the 12 xenoliths analysed in this work are spinel lherzolites, many of them containing amphibole. A summary of information on the samples is provided in Table 1 of the accompanying paper (Ionov *et al.*, 2002). We adopt here the classification of the xenoliths from that paper based on primitive mantle (PM)-normalized trace element patterns in whole rocks and minerals. Type-1 samples (in most cases without amphibole) have nearly flat heavy REE (HREE) to middle REE (MREE) patterns, moderate depletion from Eu to Nd, and a steep La–Ce–(Pr) inflection. Type-2 samples, generally containing amphibole, have lower HREE abundances and exhibit a continuous increase in normalized REE from Ho to Ce. Clinopyroxene and amphibole of both types have small to moderate positive Sr anomalies. All amphiboles are low in Rb, with Rb/Sr ratios below those of the primitive mantle (Hofmann, 1988).

Type-1 xenolith 39-86-1 is heterogeneous, with several clinopyroxene grains yielding a range of trace element abundances (Ionov *et al.*, 2002). Harzburgite 26a and lherzolite 63-90-30 cannot be grouped with either Type-1 or Type-2 samples. Sample 26a has low abundances of the lithophile trace elements and a nearly flat REE distribution pattern; 63-90-30 has a concave-upwards REE pattern. Composite xenolith 4-90-1 contains coarse amphibole and phlogopite and is probably part of a vein; its clinopyroxene and amphibole have REE patterns resembling those of the Type-2 samples.

ANALYTICAL PROCEDURES

Samples for radiogenic isotope analyses were processed using standard dissolution and column procedures described by Mukasa *et al.* (1987, 1991). Each sample was dried to a solid, treated with a drop of 14 N HNO_3, redried, and then loaded on appropriate filaments (single rhenium for Pb, Sr, and Rb, and triple rhenium for Nd and Sm). Lead was loaded with a silica gel–phosphoric acid solution, Sr with tantalum tetrachloride, and Rb, Sm, and Nd with a 10% nitric acid solution. The samples were run on VG Sector thermal ionization mass spectrometers at the University of Michigan. Lead isotopic compositions are corrected for fractionation using a factor of 0·12 ± 0·02% per atomic mass unit (a.m.u.), based on replicate analyses of National Institute of Standards and Technology (NIST) Standard NBS-981. A selected number of samples were run for Pb isotopic compositions in duplicates to confirm reproducibility. Nd and Sr ratios were normalized to $^{146}Nd/^{144}Nd = 0{\cdot}721900$ and $^{86}Sr/^{88}Sr = 0{\cdot}119400$, respectively. Measurements for the NIST Standard SRM-987 gave $^{87}Sr/^{86}Sr = 0{\cdot}710245 \pm 10$, and for the La Jolla Nd Standard $^{143}Nd/^{144}Nd = 0{\cdot}511842 \pm 10$. Total blanks averaged 0·04 ng for Pb, 0·02 ng for Nd, 0·02 ng for Sm, 0·07 ng for Rb and 0·1 ng for Sr.

Sr–Nd ISOTOPIC COMPOSITIONS

Sr–Nd–Pb isotope data are given in Table 1 and illustrated in Figs 2–4. Minerals from Type-1 xenoliths have more radiogenic $^{143}Nd/^{144}Nd$ ratios and less

Table 1: Sr–Nd–Pb isotopic analyses; concentrations (in ppm) were determined by isotope dilution for minerals and by solution ICP-MS for the basalts

Sample no.	Rb	Sr	1/Sr	$^{87}Rb/^{86}Sr$	$^{87}Sr/^{86}Sr$	Sm	Nd	1/Nd	$^{147}Sm/^{144}Nd$	$^{143}Nd/^{144}Nd$	2σ	U	Pb	$^{238}U/^{204}Pb$	$^{206}Pb/^{204}Pb$	$^{207}Pb/^{204}Pb$	$^{208}Pb/^{204}Pb$
Type 1 lherzolites																	
315-6 cpx	0·0009	171·1	0·006	1·6E – 05	0·70342	1·05	2·80	0·36	0·226	0·513378	16	0·206	0·489	27·0	18·840	15·518	38·59
315-6 amph	n.d.	n.d.			0·70342	n.d.	n.d.	n.d.		n.d.					18·705	15·506	38·50
39-86-1 cpx	n.d.	n.d.			0·70355	n.d.	n.d.	n.d.		0·513072	18			16·4	18·296	15·438	38·30
39-86-2 cpx	0·0019	70·8	0·014	7·8E – 05	0·70249	1·25	3·22	0·31	0·235	0·513594	14	0·108	0·406		17·822	15·377	37·62
4-25-90 cpx	0·0033	174·9	0·006	5·3E – 05	0·70341	1·63	5·57	0·18	0·177	0·513302	14		1·173		18·668	15·516	38·47
4-36-90 cpx	0·0042	205·1	0·005	5·9E – 05	0·70360	1·46	5·57	0·18	0·159	0·513248	15		0·698		18·047	15·369	37·85
63-90-18 cpx	0·0012	91·7	0·011	3·8E – 05	0·70315	1·26	3·09	0·32	0·247	0·513520	10	0·096	0·368	18·6	17·985	15·417	37·94
Type 2 peridotites																	
311-9 cpx	0·0008	260·1	0·004	9·0E – 06	0·70405	3·16	15·3	0·07	0·125	0·512742	24	0·153	0·319	30·3	18·279	15·444	38·26
318 cpx	0·0021	367·4	0·003	1·7E – 05	0·70399	3·23	16·6	0·06	0·118	0·512757	23			7·86	17·898	15·373	37·80
318 amph	n.d.	n.d.			0·70400	n.d.	n.d.	n.d.		0·512761	22				17·882	15·371	37·78
318-1 cpx	0·0127	331·8	0·003	0·0001	0·70400	2·30	12·9	0·08	0·108	0·512849	17		0·232		18·326	15·408	38·10
Other peridotites																	
26a cpx	0·0064	13·6	0·073	0·0014	0·70363	0·133	0·658	1·52	0·122	0·512330	17				18·529	15·449	38·19
63-90-30 cpx	0·0011	55·0	0·018	5·9E – 05	0·70319	1·91	4·89	0·20	0·236	0·512971	11	0·034	0·168	12·5	17·763	15·366	37·42
Vein																	
4-90-1 cpx	n.d.	n.d.			0·70395	n.d.	n.d.	n.d.		0·512904	23				18·474	15·495	38·32
4-90-1 phl	408·9	314·1	0·003	3·75	0·70411	0·028	0·12	8·3	0·139	0·512883	20		0·910		18·484	15·516	38·38
4-90-1 amph	17·9	834·4	0·001	0·062	0·70400	5·28	25·4	0·04	0·126	0·512894	23	0·068	0·962	4·47	18·503	15·524	38·44
Host basalts																	
1-25-90 bas	49·3	1118	0·0009	0·127	0·703700	8·28	42·9	0·023	0·117	0·512968	21	2·07	5·6		18·003	15·445	37·838
3-15-90 bas	51·9	1174	0·0009	0·127	0·703849	8·62	44·6	0·022	0·117	0·512947	22	2·21	6·2		17·986	15·433	37·794
35 bas	49·8	1076	0·0009	0·133	0·703534	8·12	41·8	0·024	0·117	0·512983	21	1·99	5·6		18·074	15·456	37·854
39-86-2 bas	50·4	1060	0·0009	0·137	0·703477	8·13	41·2	0·024	0·119	n.d.		1·99	5·5		18·038	15·44	37·804

n.d., not determined. Typical $^{87}Sr/^{86}Sr$ error is 0·00002. Reproducibility of Pb ratios is ±0·10% per a.m.u. Cpx, clinopyroxene; amph, amphibole; phl, phlogopite.

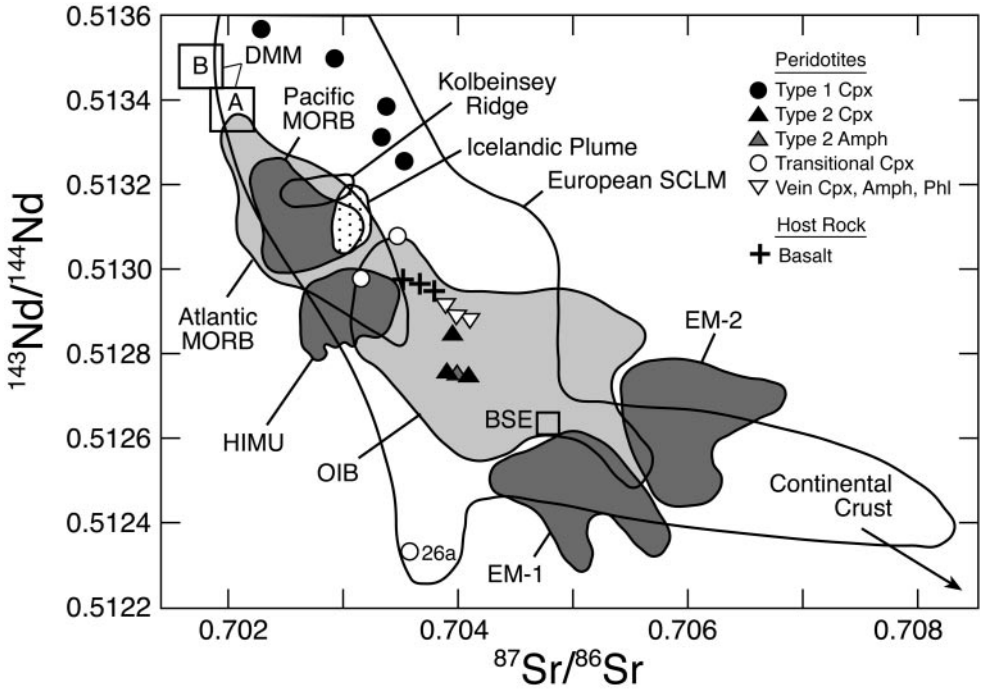

Fig. 2. Sr–Nd isotope variation diagram. Also shown are the fields of oceanic basalts and model mantle end-members (Zindler & Hart, 1986; Hofmann, 1997), and of European lithospheric mantle (SCLM) (Downes, 2001). A and B are two distinct DMM fields as defined by Zindler & Hart (1986).

radiogenic $^{87}Sr/^{86}Sr$ ratios than minerals from Type-2 xenoliths (Fig. 2). Therefore, xenolith types originally identified from trace element compositions also turn out to have distinct Sr–Nd isotopic ratios. The highly radiogenic Nd isotopic compositions of Type-1 xenoliths reflect ancient depletion of their lithospheric source in incompatible elements. Three out of five samples have $^{143}Nd/^{144}Nd$ ratios higher than Atlantic mid-ocean ridge basalt (MORB), but fall within the DMM range of Zindler & Hart (1986). All Type-1 samples are displaced to the right of the mantle array on the Nd vs Sr isotope covariation diagram (Fig. 2) and appear to contain a component anomalously enriched in radiogenic Sr. Within Eurasia, this characteristic has been observed previously in rare xenoliths from the Massif Central (Downes & Dupuy, 1987; Zangana *et al.*, 1997), Hungary (Rosenbaum *et al.*, 1997), Mongolia (Ionov *et al.*, 1994; Wiechert *et al.*, 1997) and eastern China (Tatsumoto *et al.*, 1992), as well as in the Pyrenean alpine peridotite massifs (e.g. Downes *et al.*, 1991; Mukasa *et al.*, 1991; Downes, 2001). Unfortunately, data for mantle xenoliths from the Laurentian fragments (Greenland and NE North America) that the Svalbard archipelago was a part of before the opening of the North Atlantic are still scarce.

The component that introduced the radiogenic Sr to Type-1 xenoliths has to be of mantle origin inasmuch as our sample preparation and analytical procedures rule out an extraneous origin. Careful handpicking followed by acid leaching of the mineral separates before the isotopic analyses is expected to have removed any grain-surface contamination, for instance from interstitial carbonates or post-eruption alteration. In addition, spot analyses of inclusion-free grains (Ionov *et al.*, 2002) have yielded Sr concentrations similar to those obtained by isotope dilution (ID) on bulk mineral separates. The trace element patterns of Type-1 minerals measured in mineral cores show positive Sr anomalies apparently hosted by the crystal lattice; the Sr/Nd ratios in all Type-1 and Type-2 minerals are higher than those of the primitive mantle. Moreover, post-eruption Sr enrichment would be present in all or in a random selection of samples—yet the anomalous Sr isotope compositions are only seen in Type-1 xenoliths.

The rest of the xenoliths fall in the OIB field (Fig. 2), with the exception of 26a which plots below the mantle array, trending toward an EMI-like end-member. Type-2 clinopyroxene and amphibole, together with those from composite xenolith 4-90-1, show a very narrow range in their $^{87}Sr/^{86}Sr$ values ($0{\cdot}70400 \pm 0{\cdot}00005$). The $^{143}Nd/^{144}Nd$ values in three Type-2 samples analysed are somewhat lower than in composite xenolith 4-90-1 and are practically identical in two samples with high (318) and low (311-9) amphibole abundances, respectively. Xenoliths 39-86-1 and 63-90-30 plot between these two major

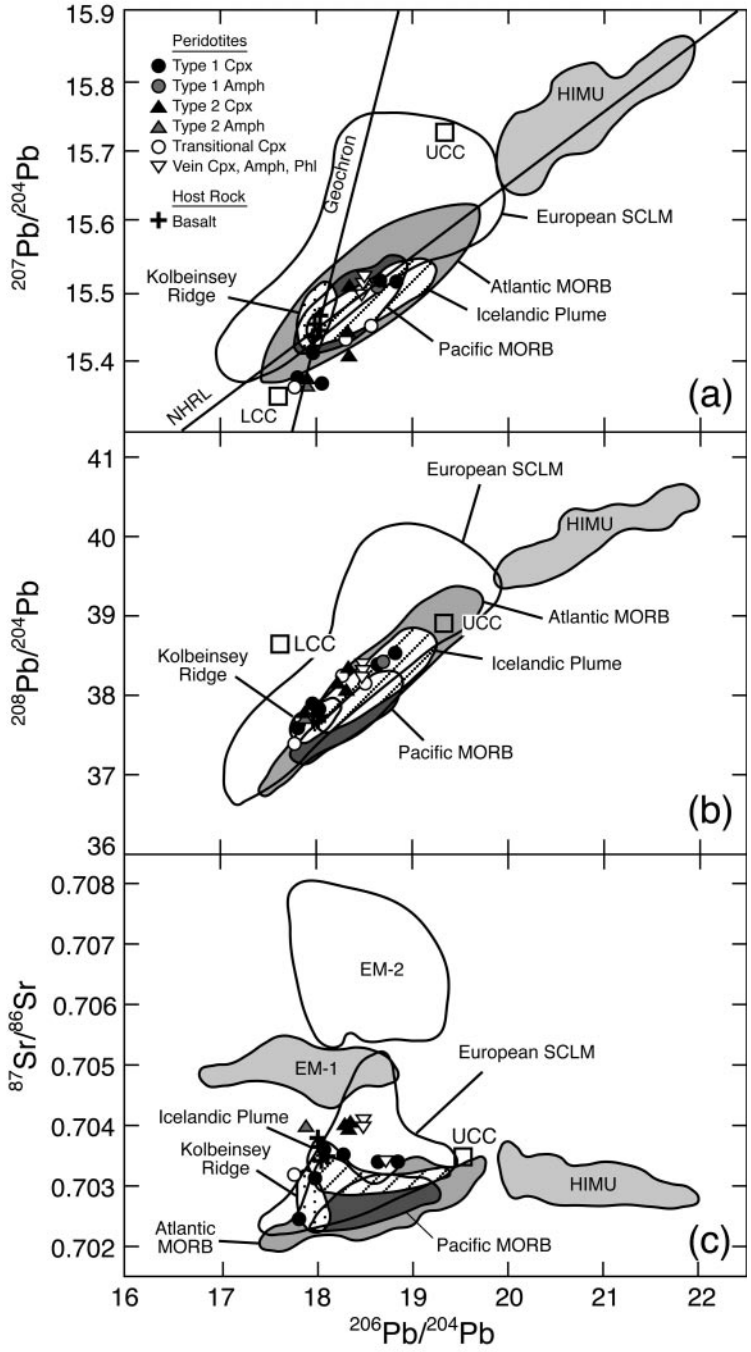

Fig. 3. Plots of $^{206}Pb/^{204}Pb$ vs (a) $^{207}Pb/^{204}Pb$, (b) $^{208}Pb/^{204}Pb$ and (c) $^{87}Sr/^{86}Sr$. Also shown are the fields of oceanic basalts and upper and lower continental crust compositions (UCC and LCC). Data sources same as in Fig. 3.

types of xenoliths and are considered here as 'transitional'. Xenolith 26a shares characteristics with the transitional group, except for its $^{143}Nd/^{144}Nd$ value, which is exceptionally low. The host basalts plot close to vein minerals from 4-90-1 and have more 'depleted' Sr–Nd isotopic compositions than the Type-2 xenoliths.

Pb ISOTOPIC COMPOSITIONS

Diagrams illustrating the Pb isotopic composition (Figs 3 and 4) show that Type-1 and Type-2 minerals are not resolvable using these data alone. Compositions of clinopyroxene are almost the same as compositions of coexisting amphibole and phlogopite (when the latter

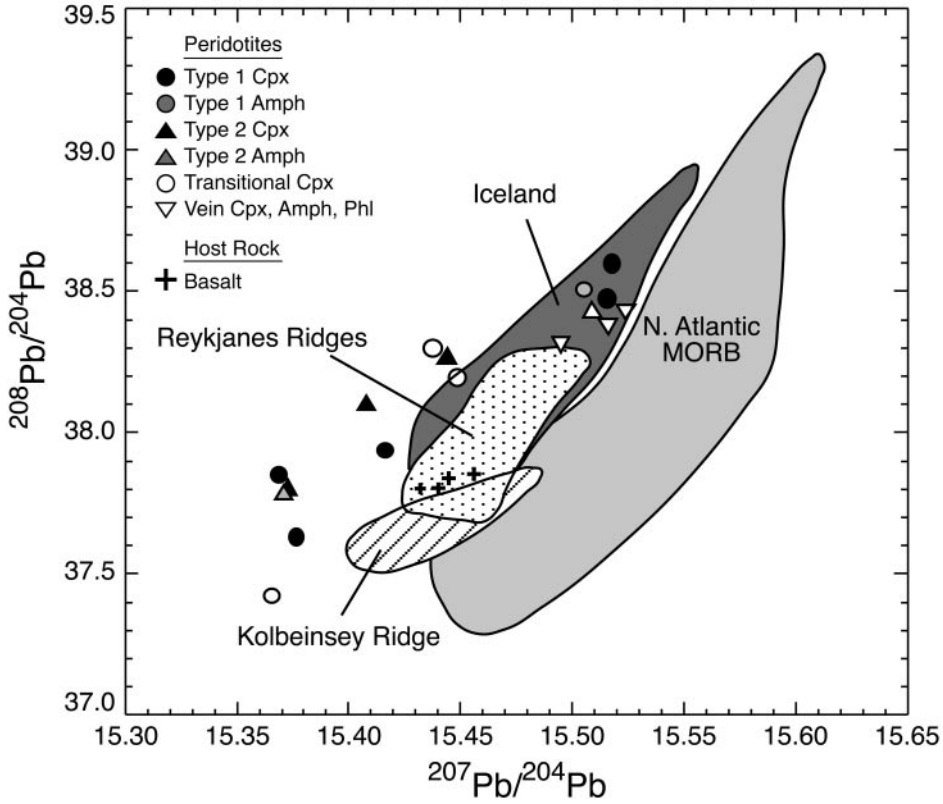

Fig. 4. A plot of $^{208}Pb/^{204}Pb$ vs $^{207}Pb/^{204}Pb$. Also shown are the fields of oceanic basalts in the vicinity of Spitsbergen (Kempton *et al.*, 2000).

two phases are present) in each individual xenolith, demonstrating nearly complete equilibration. All the mineral compositions plot as a poorly defined array on the $^{207}Pb/^{204}Pb$ vs $^{206}Pb/^{204}Pb$ diagram (Fig. 3a) that subparallels the Northern Hemisphere Reference Line (NHRL) of Hart (1984). They extend from the middle of the Atlantic MORB field to the least radiogenic end of the MORB field and beyond, where they exhibit exceptionally low $^{207}Pb/^{204}Pb$ values. These low ratios have been reproduced for a few of the samples analysed in duplicates. On the $^{208}Pb/^{204}Pb$ vs $^{206}Pb/^{204}Pb$ diagram (Fig. 3b) the xenoliths define a field that partly overlaps the Atlantic MORB field, but is displaced to $^{208}Pb/^{204}Pb$ values higher than MORB for a given value of $^{206}Pb/^{204}Pb$. The range of Pb isotopic compositions in the Spitsbergen xenoliths partly overlaps values for the Iceland plume in both $^{207}Pb/^{204}Pb$ vs $^{206}Pb/^{204}Pb$ and $^{208}Pb/^{204}Pb$ vs $^{206}Pb/^{204}Pb$ space, but only with respect to $^{208}Pb/^{204}Pb$ vs $^{206}Pb/^{204}Pb$ values in the Kolbeinsey Ridge (Kempton *et al.*, 2000, and references therein). The host basalts plot within the arrays defined by the xenoliths. Between the two plots (Fig. 3a and b) it is evident that overall, the Spitsbergen xenoliths have fairly unradiogenic uranium-derived Pb isotopes (i.e. $^{206}Pb/^{204}Pb < 19$ and $^{207}Pb/^{204}Pb < 15{\cdot}53$) seemingly akin to MORB. However, Fig. 4 highlights the fact that $^{208}Pb/^{204}Pb$ for given values of $^{207}Pb/^{204}Pb$ is considerably higher in the Spitsbergen xenoliths than in North Atlantic MORB. In this respect, they resemble basalts from the Iceland plume and Reykjanes and Kolbeinsey ridges, but extend to even less radiogenic $^{207}Pb/^{204}Pb$ values. The Spitsbergen host basalts generally share these characteristics, but plot to the right of the xenolith field in Fig. 4.

There is no overlap in Nd–Sr space, however, between any of the Spitsbergen samples and the fields for the Iceland plume and nearby Kolbeinsey Ridge from Kempton *et al.* (2000) (Fig. 2). Divergence from the MORB field is also displayed in Fig. 3c, which illustrates that the $^{87}Sr/^{86}Sr$ values of the xenoliths are considerably higher at given $^{207}Pb/^{204}Pb$ values. The latter is consistent with high Sr/Pb values (relative to PM) in the clinopyroxene and amphibole in nearly all xenoliths (Fig. 5a), possibly as a result of enrichment in Sr with little effect on Pb during metasomatism. Overall, the Sr–Nd–Pb isotopic signatures of the Spitsbergen xenoliths are distinct from those of their host basalts, North Atlantic MORB and Iceland plume basalts. This indicates, in particular, that the metasomatism that affected the Spitsbergen xenolith suite is not directly related to the source regions of the Cenozoic basalts.

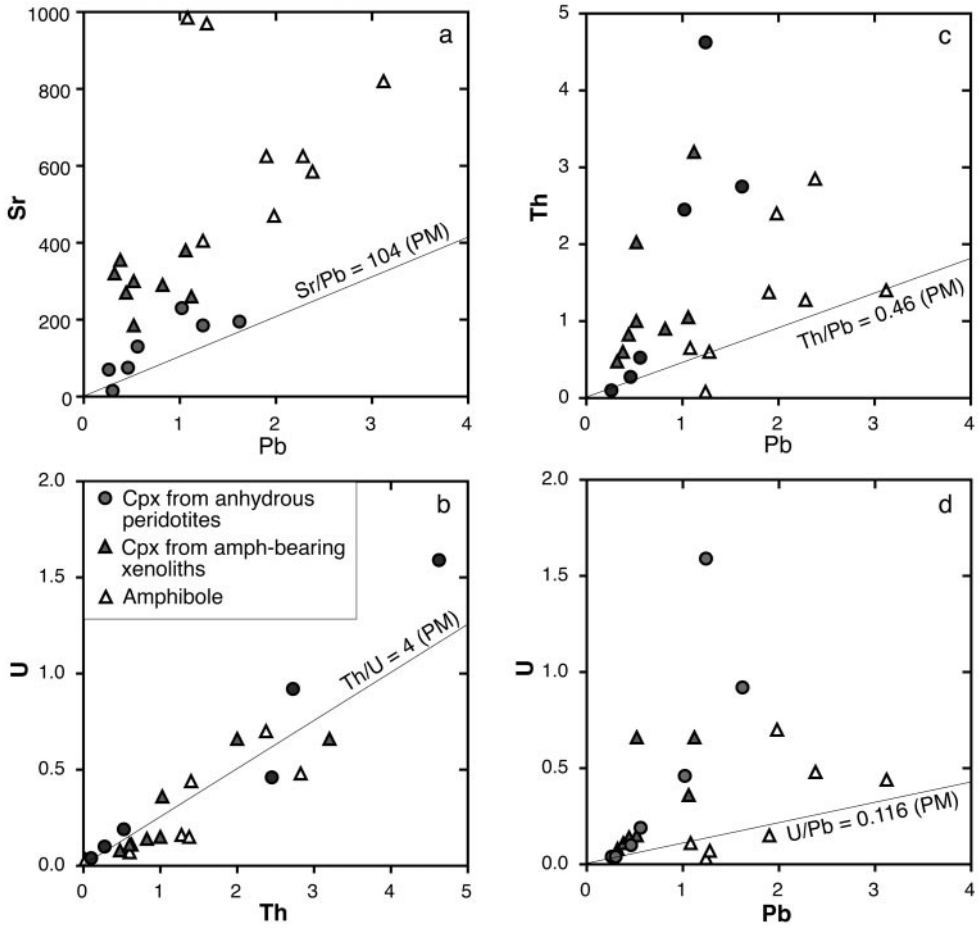

Fig. 5. Pb–Th–U–Sr covariation plots for clinopyroxene from amphibole-bearing (▲) and 'anhydrous' (●) peridotites and for amphibole (△). Data are from Ionov *et al.* (2002). Straight lines mark elemental ratios in the primitive mantle (PM) (Hofmann, 1988).

The Pb-isotope signatures imply a time-integrated record of moderate U/Pb and Th/Pb, but high Th/U in the Spitsbergen lithospheric mantle and in the source components for the basalts. By comparison, the Th/U values in the clinopyroxene and amphibole (Fig. 5b) are similar to those in the primitive mantle whereas U/Pb and Th/Pb are typically higher than in the primitive mantle (Figs. 5c and d).

Collectively, the $^{143}Nd/^{144}Nd$ vs $^{87}Sr/^{86}Sr$ signature of the Spitsbergen xenoliths fits within the fields for the European continental lithospheric mantle (CLM) (Downes, 2001) and the North American data summarized by Menzies (1990). Although completely within the field for European CLM on the $^{208}Pb/^{204}Pb$ vs $^{206}Pb/^{204}Pb$ plot, Pb isotopic ratios place most of the Spitsbergen samples outside of this field on the $^{207}Pb/^{204}Pb$ vs $^{206}Pb/^{204}Pb$ diagram. In this regard (low $^{207}Pb/^{204}Pb$ ratios), the Spitsbergen xenoliths are similar to the much larger collection from several localities in China (Tatsumoto *et al.*, 1992). A study of peridotite xenoliths from the Massif Central (Zangana *et al.*, 1997) found non-radiogenic Pb isotope compositions in LREE-depleted samples and rather radiogenic compositions ($^{206}Pb/^{204}Pb > 19{\cdot}2$; $^{208}Pb/^{204}Pb > 38{\cdot}9$) in LREE-enriched samples, but the Spitsbergen xenoliths do not show similar relationships between REE patterns and Pb isotope compositions.

DISCUSSION

Age constraints from the isotope data

Chemical data indicate that the Spitsbergen xenoliths were originally formed as residues after melt extraction (Ionov *et al.*, 2002). The REE patterns in the mildly metasomatized Type-1 samples, apart from La–Ce–(Pr) inflections, seem to preserve the record of a melting event. The age of that event may, therefore, be constrained from the Sm–Nd isotopic system. Clinopyroxenes in xenoliths 39-86-2 and 63-90-18 have the smallest LREE enrichments and account for $\geq 90\%$ of the Sm and Nd in

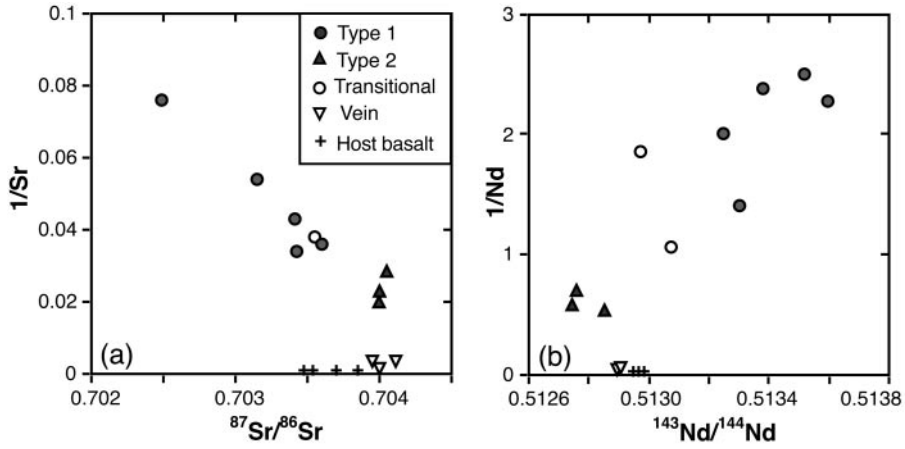

Fig. 6. Plots of 1/Sr vs $^{87}Sr/^{86}Sr$ (a) and of 1/Nd vs $^{143}Nd/^{144}Nd$ (b) for whole-rock Spitsbergen xenoliths. Sr and Nd concentrations and modal abundances used in calculations are from Ionov *et al.* (2002). Symbols are the same as in Fig. 2.

the whole rocks. Nd model ages for these two samples are very old (2·2–3·6 Ga relative to a depleted mantle source and 2·6–3·8 Ga relative to PM). The use of the Sm/Nd value obtained by laser-ablation for sample 39-86-2 instead of the ID value reduces the maximum age estimates from 3·6–3·8 to 2·3–2·6 Ga. The Sr model age for clinopyroxene 39-86-2 (the only Type-1 sample that has no Sr spike) is old as well (1·8 Ga).

Caution should be exercised while using those model age estimates, in particular considering the small number of samples and evidence for LREE metasomatism in the xenoliths. It cannot be ruled out that the metasomatism may have produced small Nd enrichments (undetectable on the REE patterns), resulting in lower Sm/Nd ratios and therefore higher model age estimates. It is beyond doubt, however, that the Sr–Nd isotope data indicate a very old, possibly Paleoproterozoic, age for depletion events that originally formed the mantle beneath Spitsbergen. Therefore, a general link with the Precambrian continental lithosphere seems reasonable. U–Pb zircon dating of metamorphic rocks and granites from Spitsbergen has given Neoproterozoic (0·62–0·66 Ga) and Grenvillian (0·94–0·97 Ga) ages (Gee *et al.*, 1995). Recent studies have also reported much older ages, from Paleoproterozoic (1·2–1·8 Ga) (Johansson & Larionov, 1999) to the less common early Paleoproterozoic and late Archean (1·8–2·1 and 2·5–2·8 Ga) (Hellman & Witt-Nilsson, 1999). In general, our results on the xenoliths indicate the formation of the lithospheric mantle beneath Spitsbergen by partial melting at roughly the same time as the formation of oldest known crustal rocks, implying a long-term mantle–crust coupling.

Assessing the age of the metasomatic event or events is complicated by the evidence for various degrees of interaction between the depleted and enriched components during metasomatism (e.g. Figs 2 and 6). When 10 of the 12 samples with complete sets of Sm–Nd data are plotted on an isochron diagram (not reproduced here), they yield an errorchron of 890 ± 250 Ma, to which it is difficult to attach any chronological significance. Furthermore, enrichment ages of individual, strongly metasomatized samples cannot be constrained by the model age approach because we cannot precisely assess either the timing of the precedent depletion event or the Nd isotopic composition of each sample at the onset of metasomatism.

The Sr and Nd isotope compositions of coexisting clinopyroxene, amphibole and phlogopite are similar or indistinguishable within analytical error. This may be due to continuing intermineral isotopic exchange until the time of host rock eruption. However, most of the samples have fairly low equilibration temperatures (e.g. 860–890°C in 315-6; 900–960°C in 318) (Ionov *et al.*, 1996, 2002), which may be too low for effective diffusion in these coarse-grained rocks. Recent experimental data on REE diffusion rates indicate closure temperatures for Nd in diopside (crystals 1 mm in diameter cooling at 1–100°C/Myr) of 960–1120°C (Van Orman *et al.*, 2002). If the minerals developed as closed systems, it follows that the formation of amphibole and phlogopite is a very young event, inasmuch as the high Rb/Sr ratios in these minerals have not yet produced significantly more radiogenic Sr isotopic ratios than in coexisting clinopyroxene. For example, the two-mineral, phlogopite–amphibole isochron for 4-90-1 (in which these two minerals are well equilibrated texturally) yields an age estimate of 2·2 ± 0·5 Ma. Moreover, even assuming effective diffusional exchange between amphibole and phlogopite, the total amphibole- and phlogopite-rich dunitic section of composite xenolith 4-90-1 would probably develop highly radiogenic Sr isotope ratios over a long period of time because of the high Rb/Sr in the

phlogopite (1·6). This, however, is not the case. Sr isotopic compositions of all minerals in sample 4-90-1 are very similar to those of Type-2 minerals that have very low Rb abundances and Rb/Sr ratios (Ionov *et al.*, 2002).

A similar argument for a relatively recent age of the metasomatism in the Spitsbergen xenoliths comes from the apparent decoupling of Pb isotopic compositions and U–Th–Pb systematics as noted in the previous section. The fairly unradiogenic Pb isotopic ratios imply a time-integrated record of moderate U/Pb and Th/Pb, and high Th/U in the source components, inconsistent with typically high U/Pb and Th/Pb and unfractionated Th/U values in the metasomatized samples (Fig. 5). Over a long period of time these trace element compositions would have produced fairly radiogenic Pb isotopic ratios. It follows that the enrichment in U and Th relative to Pb, with PM-like Th/U values, is a relatively recent event.

Evidence for peridotite–melt interaction in the Sr–Nd isotopic variations

An unusual feature of Type-1 xenoliths is that they plot to the right of the DM and MORB fields on Sr–Nd isotopic covariation diagrams and form an array between the DM end-member and the Type-2 xenoliths in the OIB field (Fig. 2). The Type-1 xenoliths can generally be interpreted as originating by different degrees of metasomatism of ancient LREE-depleted mantle, with stronger enrichment in Sr than in Nd (trace element patterns of nearly all samples have positive Sr anomalies; Ionov *et al.*, 2002). Following the line of reasoning used in the accompanying paper where we explored the origin of the trace element patterns in these xenoliths, one can try to explain the observed Sr–Nd isotope relationships either as the result of metasomatic processes or as resulting from an unusual composition of the metasomatic agent. In the latter case the source of the metasomatic components must have been enriched in radiogenic Sr and was relatively poor in Nd (i.e. had high Sr/Nd).

All Type-1 and Type-2 xenoliths (as well as one 'transitional' sample) define a good linear correlation on the plot of whole-rock 1/Sr vs $^{87}Sr/^{86}Sr$ (Fig. 6a). Notably, the host basalts (and vein minerals) plot off that trend, emphasizing (together with Nd isotope data) that the enriched metasomatic source was not identical to that of the basalts or to the melt that produced vein 4-90-1. Such linear trends are commonly considered as evidence for simple mixing, but theoretical modelling has indicated that similar correlations can alternatively be produced by melt percolation (Navon & Stolper, 1987; Reiners, 1998). Type-1 and Type-2 xenoliths yield a linear correlation also on the plot of 1/Nd vs $^{143}Nd/^{144}Nd$, but with more scatter around the trend (Fig. 6b). The fact that both Type-1 and Type-2 xenoliths plot on the same linear trends further supports the deduction made in the accompanying paper from chemical data and their numerical modelling that the two types of metasomatized xenoliths were probably formed in the same event and by the same process. On the other hand, the diffuse 1/Nd vs $^{143}Nd/^{144}Nd$ correlation for Type-1 xenoliths compared with the more regular 1/Sr vs $^{87}Sr/^{86}Sr$ trend may indicate some decoupling of the Sr and Nd isotopic systems. Because the three Type-2 samples provide a tight cluster in Fig. 6a and b, they probably approach isotopic and chemical equilibrium with the metasomatic melt or fluid.

To further explore whether mixing processes in the mantle can cause the displacement of the Sr–Nd isotopic compositions of metasomatic Spitsbergen peridotites to the right of the mantle array, we calculated the compositions of simple mixing products between a hypothetical depleted peridotite and an enriched source with variable Sr/Nd (Fig. 7). The model depleted peridotite has 10% clinopyroxene and contains 4 ppm Sr and 0·3 ppm Nd (Sr/Nd = 13·3), consistent with a residue of about 5% partial melting of a primitive spinel lherzolite ($Sr/Nd_{PM} \sim 15·5$; Hofmann, 1988; Sun & McDonough, 1989). It is very similar to the 'fertile' LREE-depleted model composition used for trace element modelling in the accompanying paper. The Sr–Nd isotopic ratios of the two end-members were selected to be slightly more 'depleted' and more 'enriched' than the least metasomatized Type-1 and most metasomatized Type-2 xenoliths, respectively. Figure 7a demonstrates that mixing between the depleted end-member and an enriched source, which has the same Sr/Nd value, obviously, produces a linear mixing line (within the mantle array). By comparison, the simple mixing models for melts with high Sr concentrations and Sr/Nd ranging from 50 to 70 (3–4 times higher than in PM) match the compositions of the Spitsbergen xenoliths fairly well (Fig. 7c and d).

Such very high Sr/Nd values (50–70), however, are not common in major types of mantle-derived volcanic rocks. Average Sr/Nd values range from 10–12 in N-type MORB to ~17 in E-type MORB and OIB (Hofmann, 1988; Sun & McDonough, 1989) and Sr/Nd is 26 in the host Spitsbergen basalts (Table 1). Examining data for some less common magmatic products from the mantle, we find that Sr/Nd values are low in major types of South African kimberlites (8–10; Smith *et al.*, 1985) and low to moderately high (≤ 30) in many other alkali-rich silicate rocks (e.g. Wilson *et al.*, 1995; Le Roex & Lanyon, 1998). Sr/Nd values in carbonatites are highly variable both within specific localities or regions (3–40 for Namibia; Le Roex & Lanyon, 1998) and in worldwide compilations (1–182; Nelson *et al.*, 1988). Extremely high Sr/Nd in some carbonatites tend to result in high average

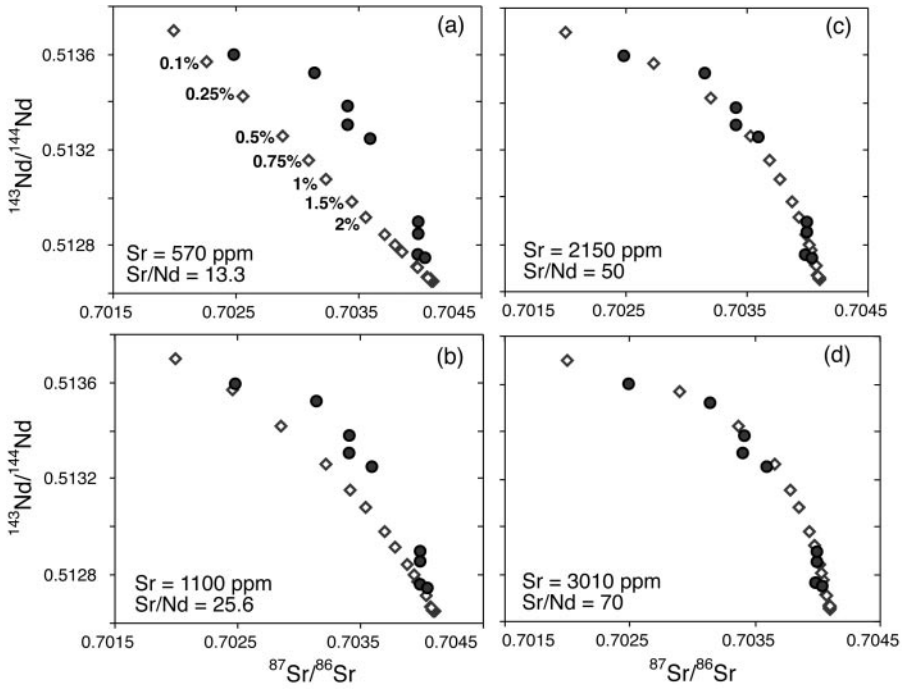

Fig. 7. Sr–Nd isotopic variation diagrams for mixing products between hypothetical depleted and enriched end-members (open rhombs) in comparison with Spitsbergen xenoliths (●). The depleted end-member is a DM-type peridotite: Sr 4 ppm, Nd 0·3 ppm, Sr/Nd = 13·3, $^{87}Sr/^{86}Sr$ = 0·702, $^{143}Nd/^{144}Nd$ = 0·5137. The enriched end-member is an OIB-type liquid with constant Nd concentration (43 ppm) and Sr–Nd isotope ratios ($^{87}Sr/^{86}Sr$ = 0·7041, $^{143}Nd/^{144}Nd$ = 0·51265), but variable Sr concentration and Sr/Nd values ranging from 570 ppm and 13·3 (a) to 3010 ppm and 70 (d), respectively.

Sr/Nd values, which may not be representative. For example, the carbonatite series from the Cape Verde and Canary Islands studied by Hoernle *et al.* (2002) has nearly equal numbers of samples with Sr/Nd < PM (0·5–15) as samples with Sr/Nd > PM (16–122), whereas an average Sr/Nd = 31 is twice as high as the PM value. It is unlikely that systematic enrichments of Sr relative to Nd are typical of carbonatite magmas in general.

Basalts and andesites of the calc-alkaline series are probably the only common magmatic rocks that have consistently high Sr/Nd. We have calculated an average Sr/Nd = 36 for Pacific rim island-arc basalts from the data of McCulloch & Gamble (1991), who attributed the relative enrichments in large-ion-lithophile elements (including Sr) in those rocks to the addition of slab-derived hydrous fluids or melts to their mantle sources. Overall, the combination of radiogenic Sr isotopic compositions and high Sr/Nd ratios in mantle-derived peridotites and volcanic rocks is commonly considered as a signature of slab-derived components (e.g. McDonough & McCulloch, 1987; Rosenbaum *et al.*, 1997; Beccaluva *et al.*, 2001).

Sr–Nd isotopic decoupling by melt percolation in peridotites

The Sr–Nd isotopic data discussed in the previous section indicate that two-component mixing of DM-type peridotites and an enriched melt with an unusually high Sr/Nd could produce displacement of the mixing products from the Sr–Nd mantle array. That model, however, does not appear to be supported by trace element data on the Spitsbergen xenoliths because (as shown in the accompanying paper) simple mixing models cannot explain the variety of trace element patterns in the metasomatized rocks. These mixing models, for example, cannot explain the distinct REE patterns and Nb/La ratios in Type-1 and Type-2 xenoliths and require multiple enriched end-members. Furthermore, the very high La/Ce and La/Nd in some Type-1 xenoliths cannot be produced by mixing of LREE-depleted peridotites with any known type of enriched mantle magmas. This is illustrated in Fig. 8, which provides a worldwide compilation of REE data for metasomatized peridotite xenoliths and strongly enriched magmatic rocks of mantle origin. The overall geochemical evidence overwhelmingly suggests that chemical fractionation processes took place

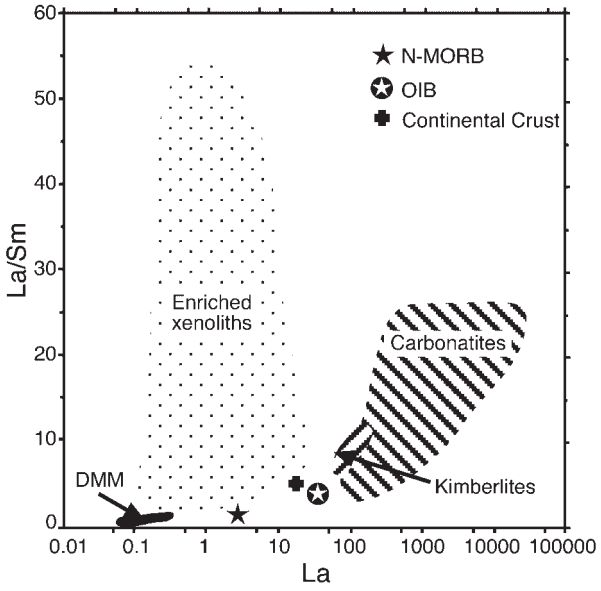

Fig. 8. A plot of La concentration (in ppm) vs La/Sm in a worldwide compilation of data on LREE-enriched xenoliths and common types of mantle-derived melts.

during metasomatism, and that this process also affected the Sm–Nd and Rb–Sr isotopic systems and is the major factor responsible for the Sr–Nd isotopic decoupling.

The chemical fractionation is caused by 'chromatographic' effects of melt percolation in the peridotite matrix, which are mainly controlled by relative magnitudes of matrix–melt partition coefficients ($D^{matrix/melt}$) for given elements (Navon & Stolper, 1987; Bodinier *et al.*, 1990). For spinel lherzolites, bulk D values for REE and Sr are largely determined by $D^{cpx/melt}$. During porous melt flow, trace element composition of melt near the percolation front becomes increasingly equilibrated with the host peridotite. However, the abundances of elements in the advancing melt change at different rates. Elements with higher cpx–melt partition coefficients are selectively removed from the melt by interaction with clinopyroxene in the host peridotite so that melt batches near the percolation front become progressively depleted in the more compatible elements relative to less compatible elements. As a result, separate chemical 'fronts' appear behind the melt percolation front, in which the concentration of a given element changes from that in the initial peridotite matrix to the one imposed by equilibrium with the initial percolating melt. Because $D^{cpx/melt}$ for Sr is lower than for Nd [see Ionov *et al.* (2002) for references], the Sr front usually advances faster than the Nd front. In the case when an enriched liquid percolates in a depleted matrix, this creates a zone where the host peridotites have experienced enrichment in Sr (with radiogenic isotopic composition) but not in Nd, thus producing Sr–Nd isotopic decoupling similar to that in moderately metasomatized Type-1 xenoliths. The Type-2 rocks may approach some degree of Sr–Nd isotopic equilibration with the percolating melts, probably as a result of high time-integrated melt/rock ratios. This may be possible if the Type-2 rocks were closer to the melt source than Type-1 rocks. Alternatively, the Type-2 peridotites may record locally higher melt flow rates or a longer duration of the infiltration process. Because the metasomatic enrichment in the xenoliths is very young, the fractionation of the parent–daughter ratios produced by percolation may not have affected the isotopic ratios significantly.

Navon & Stolper (1987) and Navon *et al.* (1996) argued on the basis of theoretical modelling that melt percolation may have consequences for isotopic compositions. Navon & Stolper (1987) noted that 1/Nd vs $^{143}Nd/^{144}Nd$ plots for percolating melt should produce straight lines, similar to a mixing line between incipient melt of the matrix and melt input into the column. The linear trend for Spitsbergen peridotites shown in Fig. 6 is therefore consistent with 'chromatographic' models. Reiners (1998) concluded that there may be decoupling of isotope systems for melts emerging from reactive melt columns. McKenzie & O'Nions (1991) and De Paolo (1996) interpreted apparently decoupled isotopic variations of Hawaiian lavas in terms of chromatographic effects.

The general concept outlined above has been tested here using numerical simulation of melt porous flow in a peridotite matrix following an approach outlined by Bodinier *et al.* (1990) and Vasseur *et al.* (1991). The method simulates melt percolation in the intergranular space of a porous matrix at a given rate until the first batch of melt arrives at a fixed distance. The model assumes mineral–melt chemical equilibration at the surface of mineral grains (considered to be spherical) and element transport in minerals by diffusion. For simplicity, trace element concentrations in the interstitial melt are considered to be homogeneous on a scale of 'Representative Elementary Volumes' (REV) because diffusion in the melt is several orders of magnitude more rapid than in the minerals (Bodinier *et al.*, 1990; Vasseur *et al.*, 1991). Similarly, isotopic ratios in the melt and the minerals are assumed to homogenize instantaneously within individual REVs. The continuous percolation is modelled as a succession of discrete steps, equivalent to individual REVs, whose size is defined using realistic time and space scales of a percolation event. Compositions of bulk peridotite, clinopyroxene and coexisting melt are listed in the modelling output for a given number of REVs when the last calculation step reaches the end of the total percolation interval. The initial Nd concentrations and Sr–Nd isotopic compositions of the matrix and the melt are the same as in simple mixing models discussed in the previous section, whereas Sr concentrations are variable. Sr–Nd isotopic decoupling

is obtained in most models for a broad range of feasible percolation parameters (porosity 0·01–2%, percolation distance 1–1000 m, percolation rate 1–100 cm/year, etc.). Modelling results plotted on Sr–Nd isotopic covariation diagrams usually yield two perpendicular nearly linear trends, one for variable $^{143}Nd/^{144}Nd$ at a given $^{87}Sr/^{86}Sr$ and vice versa, with an abrupt step-wise transition at their junction. However, the models also produce smooth curvilinear trends at certain combinations of Sr and Nd abundances in the melt and matrix, which we explored in more detail.

The numerical simulation results are presented here as two series of individual models that consider Sr–Nd isotopic compositions of metasomatized peridotites as a function of variable initial Sr concentrations either in the peridotite (Series A in Fig. 9) or in the percolating melt (Series B in Fig. 10). In both series, the distribution of Nd isotopic compositions along the percolation distance (section 1) is fixed, whereas the distribution of Sr isotopic compositions (section 2a–f) varies. In each case, the part of the percolation column on the side of the melt source has Sr and Nd isotopic compositions equilibrated with the percolating melt. In contrast, the Sr–Nd isotopic composition in the peridotite at the opposite side of the column has remained unchanged because the melt near the percolation front has equilibrated with the depleted peridotite host during porous flow. There is a transition zone where the isotopic compositions (as well as element abundances) change from those in the depleted initial matrix to those in equilibrium with the enriched initial melt. The position of this zone depends on the relative Sr (or Nd) abundances in the peridotite and in the melt (as well as on the magnitude of the differences between their isotopic compositions). Melts with higher Sr (or Nd) have greater capacity to modify the isotope composition of that element in the matrix. Inversely, peridotites with higher Sr (or Nd) are more likely to strongly 'buffer' their isotopic compositions in the melt.

When the positions of the transition zones within the percolation column coincide for Sr and Nd, the mixing lines on the corresponding Sr–Nd isotope covariation plots (section 3a–f) are curvilinear and some are very similar to those for the Spitsbergen xenoliths (Figs 9d and 10d). In general, higher Sr/Nd ratios in the initial melt relative to the matrix yield metasomatized peridotite compositions above the Sr–Nd mantle array whereas the opposite matrix–melt relationships result in compositions below the melt array (the latter may be relevant to xenolith 26a, Fig. 2). It is possible therefore to explain the whole range of Sr–Nd isotopic compositions in the Type-1 and Type-2 Spitsbergen xenoliths by a single large-scale metasomatic event assuming that xenoliths with different Sr–Nd relationships 'sample' different zones in multiple percolation systems generated within a mantle domain cross-cut by magmatic veins.

There are several significant differences between the models of metasomatism by simple mixing and by porous melt flow. In general, relative variations in Sr/Nd between matrix and melt affect the shapes of the Sr–Nd isotopic mixing lines to a much greater extent in the percolation models than in simple mixing models (compare Fig. 7 with Figs 9 and 10). Furthermore, because Sr is less compatible than Nd, melt porous flow produces relative enrichments in radiogenic Sr at lower Sr/Nd than simple mixing. As a result, Sr–Nd isotopic decoupling above the mantle array appears to be a nearly ubiquitous consequence of metasomatism by melt porous flow because enriched melts commonly have higher Sr/Nd than depleted peridotites. Remarkably, model *d* in Fig. 10 has yielded Sr–Nd isotopic relationships matching those in the Spitsbergen xenoliths at a very low Sr/Nd in the melt (14), compared with Sr/Nd in the initial matrix (13·3) and in PM (15·6). We conclude that Sr–Nd isotopic decoupling in metasomatized peridotites may not require a source with unusually high Sr/Nd, but can be a common result of metasomatism by porous flow of melts with moderate Sr/Nd values.

Pb isotope compositions do not appear to have been consistently affected by the metasomatism because they have similar ranges in the least metasomatized and most metasomatized Spitsbergen xenoliths (Figs 3 and 4). In cases when metasomatism affects Pb isotopes and the compositions of the initial peridotite and the metasomatic melt can be identified, the approach used here could be applied to explore relationships between Pb and Sr–Nd isotopic compositions during porous melt flow. However, the modelling strongly relies on good knowledge of relevant mineral–melt partition coefficients, a major factor controlling the chromatographic effects, which appear to be less well constrained and may be more affected by melt–fluid compositions for Pb than for Sr and Nd.

Character of the metasomatic source regions based on radiogenic isotope data

Several cases of Sr–Nd isotopic decoupling in mantle peridotites reported earlier in the literature were considered to represent depleted lithospheric mantle that has been enriched by metasomatic interaction with a fluid containing seawater-derived components. It was argued that those fluids derived by dehydration of subducted oceanic crust would both have high Sr/Nd and be enriched in radiogenic Sr. Such an explanation was proposed for some peridotite xenoliths from eastern China (Tatsumoto *et al.*, 1992) and Mongolia (Ionov *et al.*, 1994; Wiechert *et al.*, 1997) that have yielded Sr–Nd isotopic compositions displaced to the right of the mantle array. Both Mongolian suites have Sr-enriched, metasomatized xenoliths; in one suite from SE Mongolia the

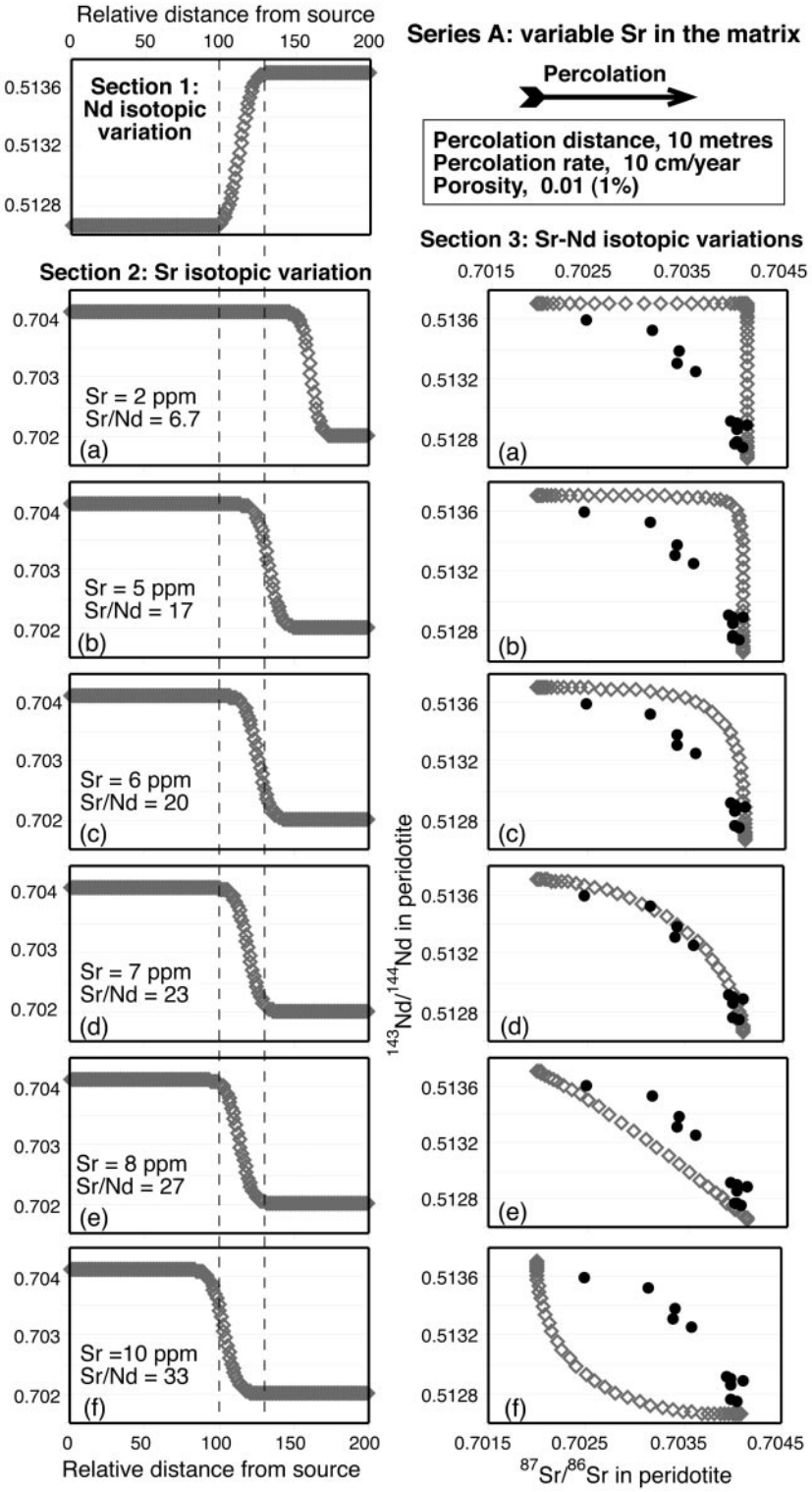

Fig. 9. Percolation Series A. Numerical simulation of Sr–Nd isotopic compositions of depleted peridotites modified by porous flow of an enriched melt (open grey rhombs) in comparison with data for Spitsbergen xenoliths (●). The depleted end-member is a DM-type peridotite (65% olivine, 23% orthopyroxene, 10% clinopyroxene, 2% spinel) with a constant Nd concentration (0·3 ppm), but variable Sr concentrations and Sr/Nd values ranging from 2 ppm and 6·7 (a) to 10 ppm and 33 (f), respectively. The enriched end-member is an OIB-type liquid with constant abundances of Nd (43 ppm) and Sr (1100 ppm), and Sr/Nd = 25·6 (see mixing model *b* in Fig. 7). Sr–Nd isotopic ratios of both end-members are the same as in Fig. 7. Partition coefficients and other modelling parameters are the same as in table 7 of Ionov *et al.* (2002).

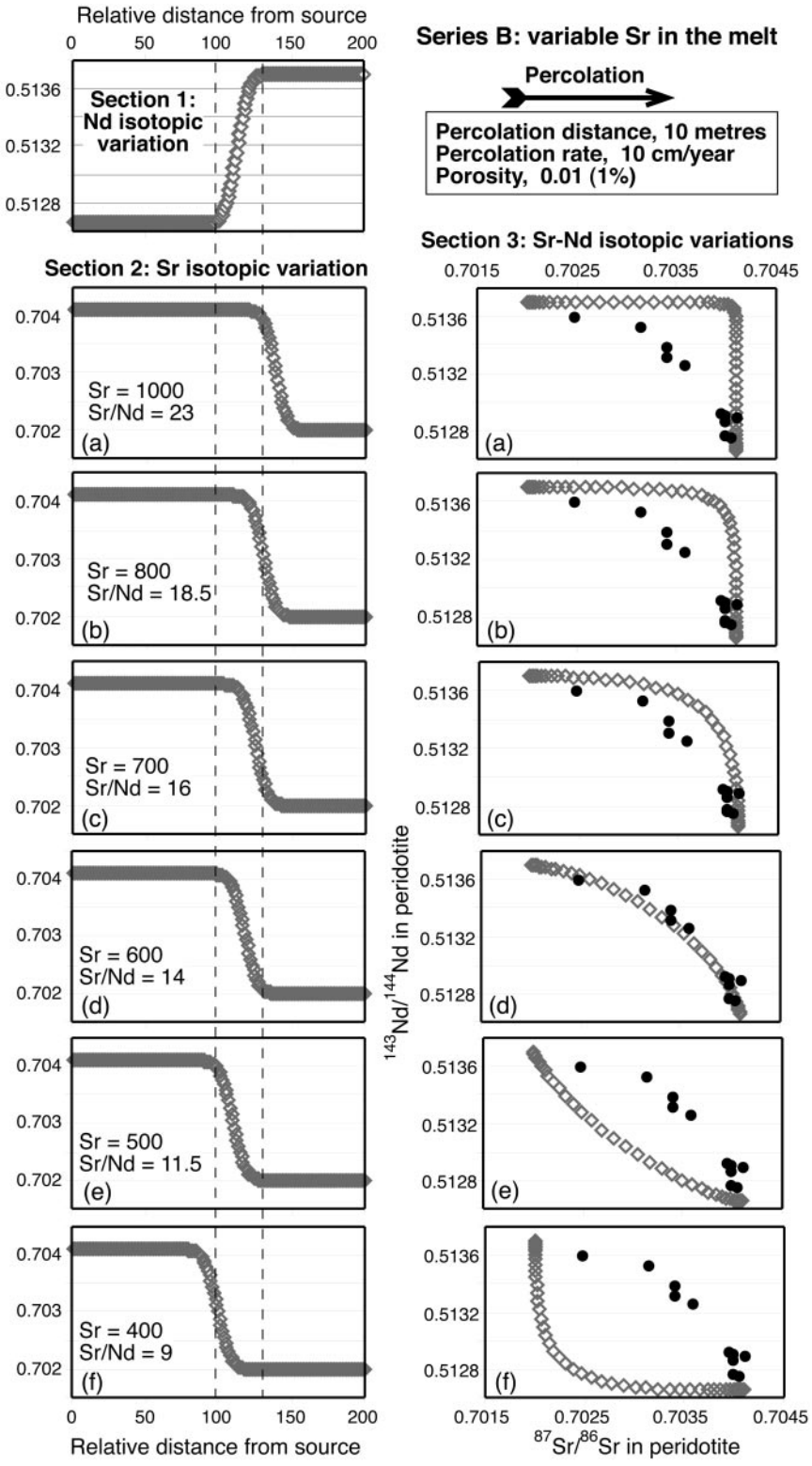

Fig. 10. Percolation Series B—same as Fig. 9. The depleted end-member is a DM-type peridotite with constant abundances of Nd (0·3 ppm) and Sr (4 ppm), and Sr/Nd of 13·3 (see mixing model *b* in Fig. 7). The enriched end-member is a liquid with constant Nd concentration (43 ppm), but variable Sr concentrations and Sr/Nd values ranging from 1000 ppm and 23 (a) to 400 ppm and 9 (f), respectively. Other parameters are the same as in Fig. 7.

samples with highly radiogenic Sr also have very high $^{34}S/^{32}S$ values, providing an additional argument for mixing with a seawater-derived source (Ionov *et al.*, 1992).

Arguably, the most remarkable case of Sr–Nd isotopic decoupling in mantle peridotites comes from a xenolith suite from western Grand Canyon (Alibert, 1994) that combines extreme Nd isotopic heterogeneity ($^{143}Nd/^{144}Nd = 0{\cdot}5127-0{\cdot}5202$) with a narrow $^{87}Sr/^{86}Sr$ range around 0·7045 and high Sr/Nd (up to 540). This variation range corresponds to the vertical branch of the Sr–Nd isotopic correlation in models *a* and *b* in Fig. 9 extended to extremely high $^{143}Nd/^{144}Nd$. The Grand Canyon xenoliths with the highest $^{143}Nd/^{144}Nd$ values have highly fractionated 'spoon-shaped' chondrite-normalized REE patterns with a steep decline from Yb to Sm followed by a sharp increase from Nd to Ce (no La data reported). These patterns are similar to those reported for some Mongolian xenoliths (Ionov *et al.*, 1994) as well as some Type-1 Spitsbergen xenoliths.

For the Spitsbergen xenolith suite, however, it is unlikely that the radiogenic Sr enrichment originated by hydrothermal alteration of the mantle lithosphere in an oceanic spreading environment, as this would require recent subduction in the area where the xenoliths are now found. Such an environment is inconsistent with the tectonic setting around Spitsbergen (Amundsen *et al.*, 1987). For such a process to apply, it would have to have been associated with an old convergent margin that is no longer active. The latter, however, is not consistent with the very young two-mineral Rb–Sr ages (<3 Ma) inferred for the amphibole and phlogopite-bearing xenoliths. Furthermore, a subduction-related source for the metasomatic events recorded in the Spitsbergen xenoliths is inconsistent with the trace element and Pb isotopic data. For example, enrichment in Pb or shifts in Pb isotope compositions (Figs 3 and 4) do not accompany the formation of amphibole and LREE enrichment. All xenolith types show similar, non-radiogenic Pb isotopic compositions and show no effects of slab-derived fluids (probably dominated by Pb derived from subducted oceanic sediments). Pb isotopic composition of some other xenolith suites inferred to have been metasomatized in subduction-related environments usually are more radiogenic (e.g. Carignan *et al.*, 1996; Rosenbaum *et al.*, 1997). More rigorous treatment of this subject, however, requires knowledge of Pb isotope composition of subducted sediments in the metasomatic source (Kempton *et al.*, 1999). In any case, a combination of depletion in Pb and enrichment in Nb found in many Spitsbergen xenoliths (Ionov *et al.*, 2002) is an unlikely feature to be found in mantle rocks metasomatized by subduction-related fluids.

We argue that Sr–Nd isotopic decoupling in mantle peridotites, with compositions displaced above the mantle array, does not necessarily require metasomatism by Sr-rich fluids generated in subduction-related environments or from ancient lithospheric mantle wedge domains affected by subduction in the past. The subduction-related provenance of the metasomatic fluid sources may indeed provide the best model in cases when other geochemical evidence supports such an origin (e.g. Vidal *et al.*, 1989; Wiechert *et al.*, 1997; Prouteau *et al.*, 2001). However, for xenolith suites from lithospheric domains without apparent links to recent or fossil subduction zones, metasomatism related to other sources (asthenospheric or lithospheric) may be a more likely option. The evidence from Spitsbergen xenoliths coupled with theoretical modelling presented here strongly indicates that percolation of OIB-type melts in ancient depleted peridotites may (and generally ought to) result in Sr–Nd isotopic decoupling. The major conclusion of this study is therefore that Sr–Nd isotopic decoupling in mantle rocks cannot generally serve as an indicator of the metasomatic source, but could alternatively be an intrinsic characteristic of the metasomatic fractionation processes.

SUMMARY

The evolution of the mantle beneath Spitsbergen can be summarized briefly as follows. The protolith for the lithospheric mantle was created by moderate degrees of melt extraction from a fertile mantle domain in the Precambrian. The source of heat and fluids for the last metasomatic episode was probably provided by a small-scale mantle plume and had general OIB geochemical characteristics. It is possible that the source of the fluids is related to the Early Cenozoic orogeny or to the thermal anomaly responsible for the eruption of late Cenozoic basalts, including those that host the xenoliths. Their sources are not identical, however. The metasomatic fluids either tapped different portions of the plume or result from high degrees of interaction between the plume-derived liquids and the base of the lithosphere.

Melts and fluids flowing in conduits penetrated into the wall rocks and propagated in them through percolation via intergranular space, which was accompanied by chromatographic effects. The resulting fractionation of elements has created a metasomatic zoning in wall-rocks, which includes Sr–Nd isotopic decoupling far from melt conduits that were 'frozen' when local sources of percolating melt were exhausted. Theoretical modelling indicates that Sr–Nd isotopic decoupling may be a common consequence of melt percolation in peridotite matrix and should not therefore in all cases be considered as a metasomatic source signature.

ACKNOWLEDGEMENTS

D.A.I. thanks Yu. Genshaft and M. Kopylova for contributing samples, H. Amundsen for advice on Spitsbergen geology, J.-Y. Cottin for assistance in St-Etienne and D. Weis for assistance in Brussels. Reviews by J. Korenaga, J. Dalton, M. Reid, R. Vannucci and an anonymous reviewer, and editorial comments by P. Kempton are highly appreciated. This research was supported by funding to D.A.I. from the Australian Research Council, Université Jean Monnet (St-Etienne, France) and Université Libre de Bruxelles, and to S.B.M. from the US National Science Foundation.

REFERENCES

Alibert, C. (1994). Peridotite xenoliths from western Grand Canyon and The Thumb: a probe into the subcontinental mantle of the Colorado Plateau. *Journal of Geophysical Research* **99**, 21605–21620.

Amundsen, H. E. F., Griffin, W. L. & O'Reilly, S. Y. (1987). The lower crust and upper mantle beneath northwestern Spitsbergen: evidence from xenoliths and geophysics. *Tectonophysics* **139**, 169–185.

Beard, B. L. & Glazner, A. F. (1995). Trace element and Sr and Nd isotopic composition of mantle xenoliths from the Big Pine volcanic field, California. *Journal of Geophysical Research* **100**, 4169–4179.

Beccaluva, L., Bianchini, G., Coltorti, M., Perkins, W. T., Siena, F., Vaccaro, C. & Wilson, M. (2001). Multistage evolution of the European lithospheric mantle: new evidence from Sardinian peridotite xenoliths. *Contributions to Mineralogy and Petrology* **142**, 284–297.

Blythe, A. E. & Kleinspehn, K. L. (1998). Tectonically versus climatically driven Cenozoic exhumation of the Eurasian plate margin, Svalbard: fission track analysis. *Tectonics* **17**, 621–639.

Bodinier, J. L., Vasseur, G., Vernières, J., Dupuy, C. & Fabriès, J. (1990). Mechanisms of mantle metasomatism: geochemical evidence from the Lherz orogenic peridotite. *Journal of Petrology* **31**, 597–628.

Carignan, J., Ludden, J. & Francis, D. (1996). On the recent enrichment of subcontinental lithosphere: a detailed U–Pb study of spinel lherzolite xenoliths, Yukon, Canada. *Geochimica et Cosmochimica Acta* **60**, 4241–4252.

Churikova, T., Dorendorf, F. & Wörner, G. (2001). Sources and fluids in the mantle wedge below Kamchatka, evidence from across-arc geochemical variation. *Journal of Petrology* **42**, 1567–1593.

De Paolo, D. J. (1996). High-frequency isotopic variations in the Mauna Kea tholeiitic basalt sequence: melt zone dispersivity and chromatography. *Journal of Geophysical Research* **101**, 11855–11864.

Downes, H. (2001). Formation and modification of the shallow subcontinental lithospheric mantle: a review of geochemical evidence from ultramafic xenolith suites and tectonically emplaced ultramafic massifs of western and central Europe. *Journal of Petrology* **42**, 233–250.

Downes, H. & Dupuy, C. (1987). Textural, isotopic and REE variations in spinel peridotite xenoliths, Massif Central, France. *Earth and Planetary Science Letters* **82**, 121–135.

Downes, H., Bodinier, J. L., Thirlwall, M. F., Lorand, J. P. & Fabriès, J. (1991). REE and Sr–Nd isotopic geochemistry of Eastern Pyrenean peridotite massifs: sub-continental lithospheric mantle modified by continental magmatism. *Journal of Petrology* **32**, 97–115.

Gee, G. G., Johansson, A., Ohta, Y., Tebenkov, A. M., Balashov, Y. A., Larionov, A. N., Gannibal, L. F. & Ryungenen, G. I. (1995). Grenvillian basement and a major unconformity within the Caledonides of Nordaustlandet, Svalbard. *Precambrian Research* **70**, 215–234.

Hart, S. R. (1984). A large-scale anomaly in the Southern Hemisphere mantle. *Nature* **309**, 753–757.

Hellman, F. & Witt-Nilsson, P. (1999). Single-zircon geochronology of metasediments and a meta-dolerite in the tectonostratigraphy of the Ny Friesland orogen, northeastern Spitsbergen. *Journal of Conference Abstracts* **4**, 594.

Hoernle, K., Tilton, G., Le Bas, M. J., Duggen, S. & Garbe-Schönberg, D. (2002). Geochemistry of oceanic carbonatites compared with continental carbonatites: mantle recycling of oceanic crustal carbonate. *Contributions to Mineralogy and Petrology* **142**, 520–542.

Hofmann, A. W. (1988). Chemical differentiation of the Earth: the relationship between mantle, continental crust, and oceanic crust. *Earth and Planetary Science Letters* **90**, 297–314.

Hofmann, A. W. (1997). Mantle geochemistry: the message from oceanic volcanism. *Nature* **385**, 219–229.

Ionov, D. A., Hoefs, J., Wedepohl, K. H. & Wiechert, U. (1992). Content and isotopic composition of sulphur in ultramafic xenoliths from central Asia. *Earth and Planetary Science Letters* **111**, 269–286.

Ionov, D. A., Hofmann, A. W. & Shimizu, N. (1994). Metasomatism-induced melting in mantle xenoliths from Mongolia. *Journal of Petrology* **35**, 753–785.

Ionov, D. A., O'Reilly, S. Y., Kopylova, M. G. & Genshaft, Y. S. (1996). Carbonate-bearing mantle peridotite xenoliths from Spitsbergen: phase relationships, mineral compositions and trace element residence. *Contributions to Mineralogy and Petrology* **125**, 375–392.

Ionov, D. A., Bodinier, J.-L., Mukasa, S. B. & Zanetti, A. (2002). Mechanisms and sources of mantle metasomatism: major and trace element compositions of peridotite xenoliths from Spitsbergen in the context of theoretical modelling. *Journal of Petrology* **43**, 2219–2259.

Johansson, A. & Larionov, A. (1999). Grenvillian and Caledonian magmatism on Nordaustlandet, Northeast Svalbard. *Journal of Conference Abstracts* **4**, 594.

Kempton, P. D., Hawkesworth, C. J., Lopez-Escobar, L., Pearson, D. G. & Ware, A. J. (1999). Spinel ± garnet lherzolite xenoliths from Pali Aike, Part 2: Trace element and isotopic evidence on the evolution of lithospheric mantle beneath southern Patagonia. In: Gurney, J. J., Gurney, J. L., Pascoe, M. D. & Richardson, S. H. (eds) *Proceedings of the 7th International Kimberlite Conference*. Cape Town: Red Roof Design, pp. 415–428.

Kempton, P. D., Fitton, J. G., Saunders, A. D., Nowell, G. M., Taylor, R. N., Hardarson, B. S. & Pearson, G. (2000). The Iceland plume in space and time: a Sr–Nd–Pb-Hf study of the North Atlantic rifted margin. *Earth and Planetary Science Letters* **177**, 255–271.

Le Roex, A. P. & Lanyon, R. (1998). Isotope and trace element geochemistry of Cretaceous Damaraland lamprophyres and carbonatites, northwestern Namibia: evidence for plume–lithosphere interactions. *Journal of Petrology* **39**, 1117–1146.

Mattielli, N., Weis, D., Scoates, J. S., Shimizu, N., Mennessier, J.-P., Grégoire, M., Cottin, J.-Y. & Giret, A. (1999). Evolution of heterogeneous lithospheric mantle in a plume environment beneath the Kerguelen Archipelago. *Journal of Petrology* **40**, 1721–1744.

McCulloch, M. T. & Gamble, J. A. (1991). Geochemical and geodynamic constraints on subduction zone magmatism. *Earth and Planetary Science Letters* **102**, 358–374.

McDonough, W. F. & McCulloch, M. T. (1987). The southeast Australian lithospheric mantle: isotopic and geochemical constraints on its growth and evolution. *Earth and Planetary Science Letters* **86**, 327–340.

McKenzie, D. & O'Nions, R. K. (1991). Partial melt distributions from inversion of rare earth element concentrations. *Journal of Petrology* **32**, 1021–1091.

Menzies, M. A. (ed.) 1990. *Continental Mantle*. Oxford: Clarendon Press.

Menzies, M. A. & Hawkesworth, C. J. (eds) 1987. *Mantle Metasomatism*. London: Academic Press.

Mukasa, S. B., McCabe, R. & Gill, J. B. (1987). Pb-isotopic compositions of volcanic rocks in the West and East Philippine island arcs: presence of the Dupal isotopic anomaly. *Earth and Planetary Science Letters* **84**, 153–164.

Mukasa, S. B., Shervais, J. W., Wilshire, H. G. & Nielson, J. (1991). Intrinsic isotopic heterogeneities exhibited by the Lherz alpine peridotite massif, French Pyrenees. *Journal of Petrology Special Volume*, 117–134.

Navon, O. & Stolper, E. (1987). Geochemical consequences of melt percolation: the upper mantle as a chromatographic column. *Journal of Geology* **95**, 285–307.

Navon, O., Frey, F. A. & Takazawa, E. (1996). Magma transport and metasomatism in the mantle: a critical review of current geochemical models—Discussion. *American Mineralogist* **81**, 754–759.

Nelson, D. R., Chivas, A. R., Chappell, B. W. & McCulloch, M. T. (1988). Geochemical and isotopic systematics in carbonatites and implications for the evolution of ocean-island sources. *Geochimica et Cosmochimica Acta* **52**, 1–17.

Prouteau, G., Scaillet, B., Pichavant, M. & Maury, R. (2001). Evidence for mantle metasomatism by hydrous silicic melts derived from subducted oceanic crust. *Nature* **410**, 197–200.

Reiners, P. W. (1998). Reactive melt transport in the mantle and geochemical signatures of mantle-derived magmas. *Journal of Petrology* **39**, 1039–1061.

Rosenbaum, J. M., Wilson, M. & Downes, H. (1997). Multiple enrichment of the Carpathian–Pannonian mantle: Pb–Sr–Nd isotope and trace element constraints. *Journal of Geophysical Research* **B102**, 14947–14961.

Smith, C. B., Gurney, J. J., Skinner, E. M. W., Clement, C. R. & Ebrahim, N. (1985). Geochemical character of southern African kimberlites: a new approach based on isotopic constraints. *Transactions of Geological Society of South Africa* **88**, 267–280.

Sun, S. S. & McDonough, W. F. (1989). Chemical and isotopic systematics of oceanic basalts: implications for mantle composition and processes. In: Saunders, A. D. & Norry, M. J. (eds) *Magmatism in the Ocean Basins*. *Geological Society, London, Special Publications* **42**, 313–345.

Tatsumoto, M., Basu, A. R., Huang, W., Wang, J. & Xie, G. (1992). Sr, Nd, and Pb isotopes of ultramafic xenoliths in volcanic rocks of eastern China: enriched components EMI and EMII in subcontinental lithosphere. *Earth and Planetary Science Letters* **113**, 107–128.

Van Orman, J. A., Grove, T. L., Shimizu, N. & Layne, G. D. (2002). Rare earth element diffusion in a natural pyrope single crystal at 2·8 GPa. *Contributions to Mineralogy and Petrology* **142**, 416–424.

Vasseur, G., Vernières, J. & Bodinier, J.-L. (1991). Modeling of trace element transfer between mantle melt and heterogranular peridotite matrix. *Journal of Petrology Special Volume*, 41–54.

Vidal, P., Dupuy, C., Maury, R. & Richard, M. (1989). Mantle metasomatism above subduction zones: trace-element and radiogenic isotope characteristics of peridotite xenoliths from Batan Island (Philippines). *Geology* **17**, 1115–1118.

Wiechert, U., Ionov, D. A. & Wedepohl, K. H. (1997). Spinel peridotite xenoliths from the Atsagin-Dush volcano, Dariganga lava plateau, Mongolia: a record of partial melting and cryptic metasomatism in the upper mantle. *Contributions to Mineralogy and Petrology* **126**, 345–364.

Wilson, M., Rosenbaum, J. M. & Dunworth, E. A. (1995). Melilitites: partial melts of the thermal boundary layer? *Contributions to Mineralogy and Petrology* **119**, 181–196.

Yevdokimov, A. N. (2000). *Volcanoes of Spitsbergen*. St Petersburg: VNIIOkeangeologija (in Russian with English abstract).

Zangana, N. A., Downes, H., Thirlwall, M. F. & Hegner, E. (1997). Relationship between deformation, equilibration temperatures, REE and radiogenic isotopes in mantle xenoliths (Ray Pic, Massif Central, France): an example of plume–lithosphere interaction? *Contributions to Mineralogy and Petrology* **127**, 187–203.

Zindler, A. & Hart, S. (1986). Chemical geodynamics. *Annual Review of Earth and Planetary Sciences* **14**, 493–571.